Mechanical properties of friction stir welded St 37 and St 44 steel joints

Tevfik Küçükömeroğlu, Trabzon, Semih Mahmut Aktarer, Rize, Güven İpekoğlu and Gürel Çam, Hatay, Turkey

Article Information

Correspondence Address
Prof. Dr. Gürel Çam
Iskenderun Technical University
Faculty of Engineering and Natural Sciences
Department of Mechanical Engineering
Iskenderun, Hatay, 31200 Turkey
E-mail: gurel.cam@iste.edu.tr

Keywords
Friction stir welding, dissimilar joint, steel St 37 and St 44, microstructure, mechanical properties

In this study, the weldability of lower strength St 37 grade steel plate with a higher strength steel plate (i. e., St 44) using the friction stir welding technique has been studied. St 37 grade steel sheets are widely used in various industries. However, the joining of St 37 steel plates with higher strength grades such as St 44 grade steel is usually required when the strength of St 37 grade is not sufficient. Therefore, microstructural and mechanical properties of friction stir welded St 37-St 44 butt joints were investigated by conducting optical microscopy, microhardness measurements, and tensile testing. A fine-grained recrystallized microstructure was observed in the weld regions of the joints produced. The highest tensile strength, i. e. 385 MPa, was exhibited by the joint produced at 630 rev × min^{-1}.

Materials Testing downloaded from www.hanser-elibrary.com by Hanser - Library on December 17, 2018
For personal use only.

A recently developed solid state welding technique, namely friction stir welding (FSW), which was developed and patented by The Welding Institute (TWI) [1], can be applied to join similar materials, such as Al-alloys [2-19], Mg-alloys [4, 6, 20], pure Pb [21], Cu-alloys [22-24], Ti-alloys [20] and steels [20, 22, 25-43] and even dissimilar materials owing to the fact that heat input is low in this process [2].

Although FSW can be successfully used in joining low melting temperature materials such as Al-alloys, the application of this technique to higher melting temperature structural materials such as steel is very limited due to the limited tool materials available which can withstand much higher temperatures experienced during the FSW of these materials [4, 20]. Lower residual stress and distortions develop in the weld region and the grain growth occurs to a lesser extent in the heat affected zone (HAZ) in FSWed structural steels due to the low heat input of the process compared to fusion joining methods. These advantages of the FSW technique have drawn the attention of researchers for the application of the method to steel [20]. Thus, several researchers investigated the weldability of carbon steels using FSW. For example, Fuji et al. [32] investigated the microstructural changes of stir zones (SZs) of FSWed ultra-low carbon (ULC) interstitial free (IF) steel plates. Fuji et al. [33] also joined three types of steel plates, i. e., IF steel, S12C steel and S35C steel, by means of the FSW technique using different weld parameters, and they found that these steels can be successfully joined at low temperatures, such as 923 K (650 °C), without any microstructural transformations occurring in the weld region.

Lienert et al. [34] have demonstrated the feasibility of FSW for joining hot-rolled AISI 1018 mild steel at travel speeds ranging from 25 mm × min^{-1} to 100 mm × min^{-1}. They have reported that the weld region displayed several microstructurally distinct regions including the stir zone, a grain-coarsened region, a grain-refined region, an inter-critical region and a sub-critical region containing partially spheroidized carbides [34]. Cui et al. [35] also successfully joined high carbon steel, i. e. S70C (0.72 wt.-% C), using FSW without any pre- or post-weld treatment operation. They have suggested two ways to obtain a sound joint for this steel grade. First, performing the weld below the A1 point and secondly, keeping the cooling rate below the critical cooling rate level. Imam et al. [36] joined a medium carbon low alloy steel using the FSW technique employing different weld parameters and reported that increasing the welding speed decreases the hardness and the volume fraction of martensite in the SZ.

Cui et al. [37] conducted the FSW of five types of ferritic-pearlitic carbon steels with different carbon contents (IF steel, S12C, S20C, S35C, S50C) using various welding parameters. They found that the peak temperature which evolves during the process decreases with increasing welding speed. On the other hand, the cooling rate increases with increasing welding speed. Also, they reported that these values are independent of the type of steel [37]. Ozekcin et al. [38] also joined medium carbon steels whose mean grain sizes are 7 µm and 20 µm using FSW. They reported that the hardness of the weld region is higher than that of the base plate and depends on the rotational rate of the tool.

The studies discussed above are related to the FSW of similar steel plates. There are very limited studies on FSW of dissimilar Fe-based materials [44]. Most industrial applications usually require joining different carbon containing steels in order to ob-

Materials Testing downloaded from www.hanser-elibrary.com by Hanser - Library on December 17, 2018
For personal use only.

tain a desirable design and to reduce the total manufacturing cost. Thus, there is a need to do further research on joining Fe-based materials which have different compositions and consequently different mechanical properties.

St 37 and St 44, which are known as structural steels, are widely used in riveted, screw-and-bolt connected and welded structures and in the production of various machine parts [45-48]. However, joining St 37 steel parts with higher strength grades such as St 44 grade steel is usually required when the strength of St 37 grade is not sufficient. This was the motivation of the current study. Thus, St 37 and St 44 steel plates which have different mechanical properties, have been joined in this study via the FSW technique at a constant welding speed using three different rotational rates. The mechanical and microstructural properties of the weld zones of the joints produced are investigated in detail.

Experimental procedure

In this study, St 37 and St 44 steel plates with dimensions of 200 × 40 × 4 mm were joined using the FSW technique. The chemical compositions of the base plates which were supplied in hot rolled condition are given in Table 1. The tool used for the weld trials has an 18 mm shoulder diameter and a conical pin with a large diameter of 7 mm, a small diameter of 5 mm and a length of 3.8 mm. The FSW tool was produced from tungsten carbide (WC). The weld trials were performed using three different rotational rates, namely 630, 800 and 1000 rev × min^{-1} at a constant welding speed of 55 mm × min^{-1} at a constant vertical force of 10 kN with a tilt angle of 3°.

The schematic illustration of the welded plates and the specimens extracted from these welded plates are given in Figure 1a. The temperature was measured throughout all the varied joining processes by placing a thermocouple in a hole drilled from underneath the St37 plate (in the middle of the joint line) near the top surface as illustrated in Figure 1b. Tensile test specimens with dimensions of 3 × 6 × 26 mm were prepared as shown in Figure 1a and tested using an electromechanical tensile test machine at a loading rate of 5.4 × 10^{-4} s^{-1}. The specimens used for the microstructural examination were extracted from all the welded plates perpendicular to the weld direction. Following the standard grinding and polishing procedure, metallography specimens were etched in 2 vol.-% nital reagent. The hardness profiles of the welded plates were obtained both in longitudinally and transverse directions at a dwell time of 10 s and a load of 2.96 N. The microstructures evolving in the weld regions of the joints were investigated in detail by optical microscopy.

Material	ASTM	C_{max}	Mn_{max}	P_{max}	Cu	N_{max}
St 37	A283C	0.17	1.40	0.035	0.55	0.012
St 44	A36	0.21	1.50	0.035	0.55	0.012

Table 1: Chemical composition (wt.-%) of the base plates used in this study

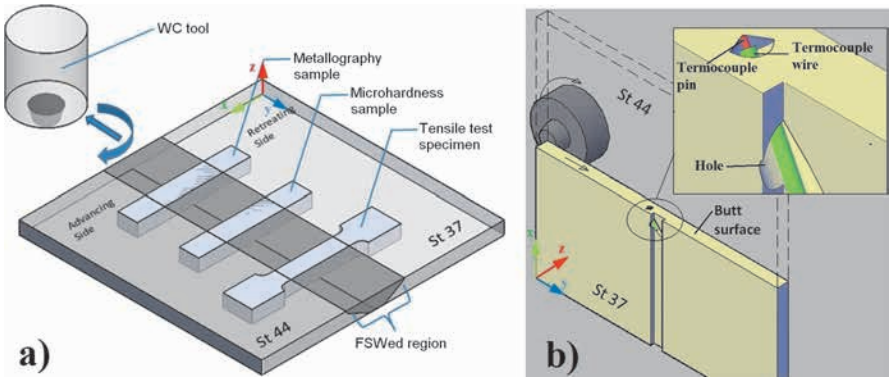


Figure 1: Schematic illustrations, a) friction stir welding (FSW) process and extraction of the specimens from the joints produced, b) location of thermocouples to measure the temperature

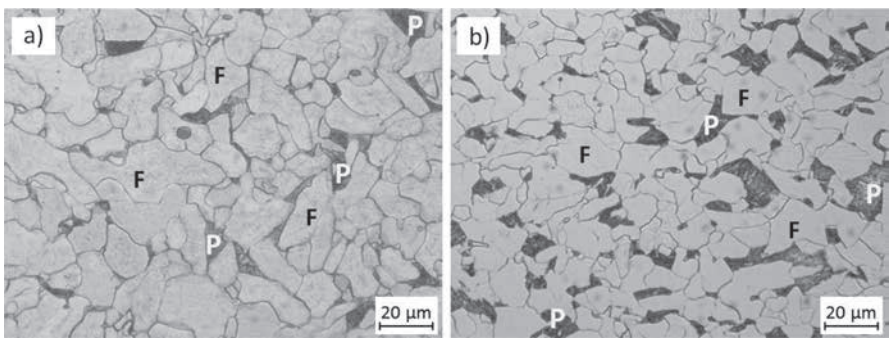


Figure 2: Optical micrographs showing the microstructures of the base plates, a) St 37, b) St 44

Results and discussion

Microstructural aspects. The microstructures of St 37 and St 44 steel plates used in this study are shown in Figure 2, and their chemical composition is listed in Table 1. The microstructure of St 37 base plate consists of equiaxed ferrite grains with an average grain size of about 13 µm and an approximately 9 % pearlite phase. On the other hand, the microstructure of St 44 base plate consists of equiaxed ferrite grains with an average grain size of about 10 µm and an approximately 17 % pearlite phase. Thus, the grain size of the microstructures of the two base plates used are quite similar. The only difference is the volume percent of the pearlite which is 8 % higher in St 44 steel.

Figure 3 shows the surface appearance of the joints produced using various rotational rates. As seen from these surface views, the joints produced at higher rotational speeds, particularly at 1000 rpm, contain some slotting defects on the surface; whereas the joint obtained at a rotational rate of 630 rpm has no surface defects. The reason for this is thought to be the excessive softening of the material as a result of higher heat input at higher rotational ratios in addition to the fact that the clamping might be inadequate at higher rotational rates.

On the other hand, the clamping was apparently adequate at a low rotation rate in addition to the lower heat input involved at this rotational rate. Thus, no slot formation took place (see Figure 3). Peak temperatures, measured from the top surface of the weld

Materials Testing downloaded from www.hanser-elibrary.com by Hanser - Library on December 17, 2018
For personal use only.

area for the joints were obtained at rotational rates of 1000 rev × min^{-1}, 800 rev × min^{-1}, and 630 rev × min^{-1} are 1433 K (1160 °C), 1318 K (1045°C), and 1203 K (930 °C), respectively. Thus, the peak temperature (i. e. 930 °C) being about 50-60 °C above the A3 temperature is the most convenient since higher temperatures than this results in the formation of coarse austenite grains during joining, which in turn negatively affect the joint properties. Therefore, the joint produced at a rotational rate of 630 rev × min^{-1} is free from any weld defect (see Figure 4a).

However, the joints obtained at rotational rates of 1000 rev × min^{-1} and 800 rev × min^{-1} contain some weld defects, i. e. tunnel defect (see Figures 4b and 4c). The formation of these defects at the joints produced at higher rotational rates are due to excessive heat generation and inadequate material flow and mixing. Similar tunnel defects were also reported in similar AISI 409M ferritic stainless steel [49] and AZ31B Mg-alloy friction stir welds [50].

Generally, a cross-section of the FSWed Al-alloys and other similar alloys joints, in which recrystallization is not easily induced, consists of four regions, namely a dynamically recrystallised zone (DXZ), a thermodynamically affected zone (TMAZ), a heat affected zone (HAZ), and an unaffected base plate region [51]. On the other hand, the cross-sections of the FSWed steels, Ti-alloys, Cu-alloys and other similar alloys in which recrystallization is easily induced, consist in contrast of only three regions, namely a DXZ, an HAZ, and an unaffected base plate. There is no visible TMAZ in the weld area of these alloys [23]. The macrograph showing the cross-section and detailed micrographs of the joint produced at a rotational rate of 630 rev × min^{-1} are shown in Figures 4a and 5a. It can be seen from the cross-sectional view of the joint that there is no weld defect in the weld region. Moreover, the characteristic onion rings can also be seen in these figures. But, since the chemical compositions and thus the microstructures of the base plates used are very similar, as seen in Table 1 and Figure 2, a visible mixing of the two mating materials which is usually observed in dissimilar FS welding was not encountered, (see Figure 4).

As clearly seen in Figures 5b and 5e, the microstructures of the DXZ and the TMAZ regions are very similar. The stir zone including the DXZ and the TMAZ has apparently undergone a plastic deformation at a relatively high temperature [34] due to the friction during FSW and the movement of the stirring tool. Thus, the microstructure of this region (DXZ and TMAZ) consists of a Widmanstatten structure comprising random and oriented ferrite grains, (see Figures 5b and 5e).

HAZ I and HAZ III regions which are the HAZ regions neighboring the TMAZ regions on either side of the stir zone consist of fully recrystallized fine ferrite and pearlite phases, (see Figures 5c and 5f). These grain refined HAZ regions transform to austenite during the joining process due to the fact that the temperature exceeds the critical temperature level (A_3), and decomposes into fine grained ferrite and pearlite phases upon cooling [48]. The average grain size in the HAZ I and III is about 7 µm for both St 37 steel (see Figure 5c) and St 44 steel sides (see Figure 5f). Figure 5d is an optical microscope image which shows the partial grain refinement in the HAZ region. This region consists of coarse ferrite grains as well as dissolved pearlite and fine ferrite grains. This critical HAZ region was exposed to a temperature between the A_1 and A_3 temperatures during welding. Moreover, a homogenization of the microstructure and a spheroidization of the cementite phases took place in those

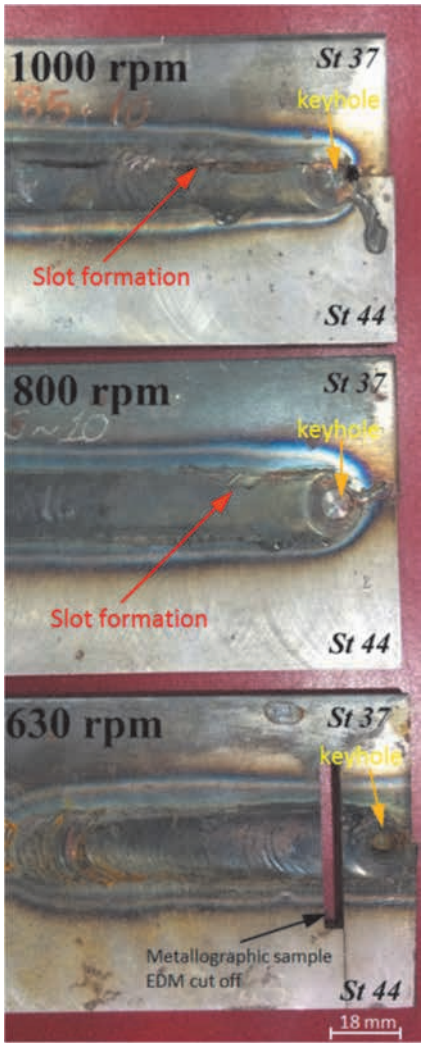


Figure 3: Macrographs showing the surfaces of the welded plates

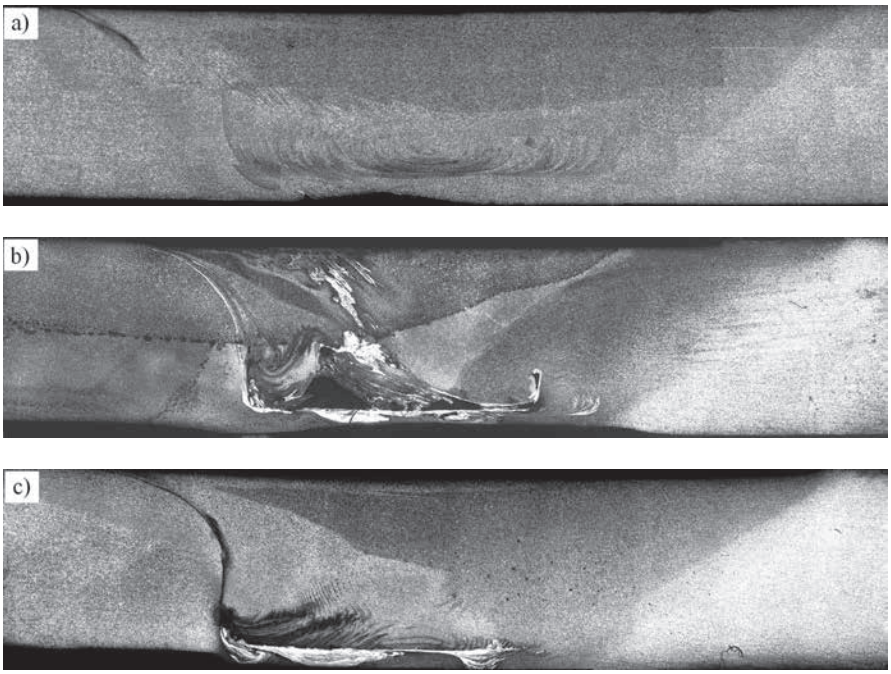


Figure 4: Optical macrographs showing the cross-sections of the three dissimilar joints obtained at different rotational rates, a) 630 rev × min^{-1} , b) 800 rev × min^{-1}, c) 1000 rev × min^{-1} (Note: The presence of weld defects in the joints produced at rotational rates of 1000 and 800 rev × min^{-1})

Materials Testing downloaded from www.hanser-elibrary.com by Hanser - Library on December 17, 2018
For personal use only.

regions (HAZ II) which were exposed to a temperature below A_1 for a sufficient time during welding as reported by several researchers [52]. As discussed above, although the TMAZ is generally visible in the weld regions of FSWed Al-alloys in which recrystallization is not easily induced [20], it is not visible in the weld region of steels such as those used in this study. Thus, it resembles the DXZ because of the occurrence of full recrystallization, (see Figure 5e). Although there is no void formation in the root region of the joint, there is a typical dark line which is about 150 µm in length, (see Figure 5 g). This seems to be a surface oxide inclusion from the surface of the anvil (backing plate). Similar contamination from the anvil was also reported in the literature for FS welds of 12 % chromium alloy steel [53]. Moreover, there is also a small groove-like defect in the root region of this joint as seen in Figures 4a and 5a which is believed to result from the plates sticking to the anvil during FSW. This defect can be readily avoided by cleaning the anvil surface prior to joining and by using an optimum plunging depth.

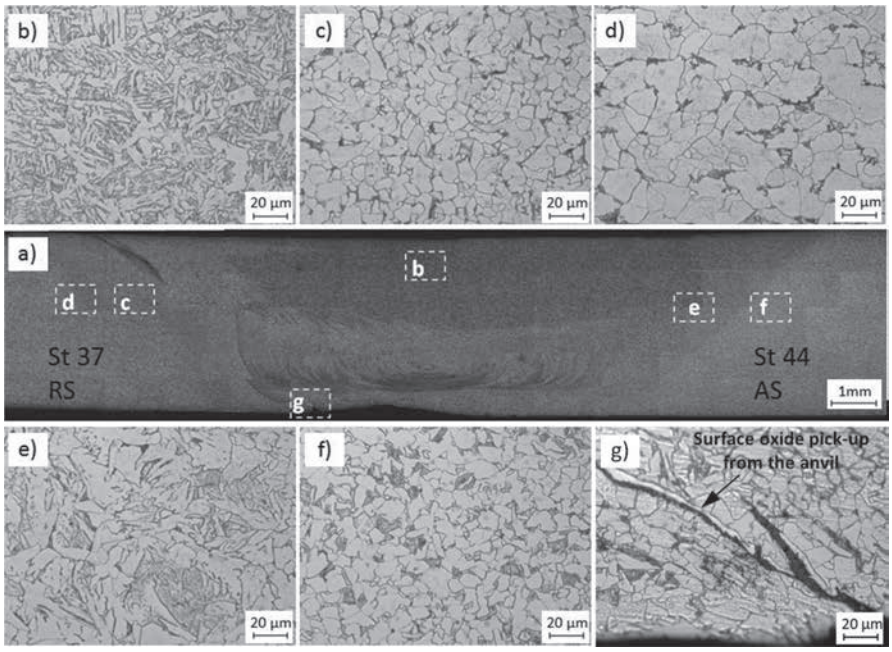


Figure 5: Optical macrographs of the FSWed joint produced at a rotating speed of 630 rev × min^{-1}, a) cross section, b) DXZ, c) HAZ I, retreating side St 37, d) HAZ II, e) TMAZ, advancing side St 44, f) HAZ III, advancing side, g) root region showing a dark line believed to be formed due to the mixture of two different steels

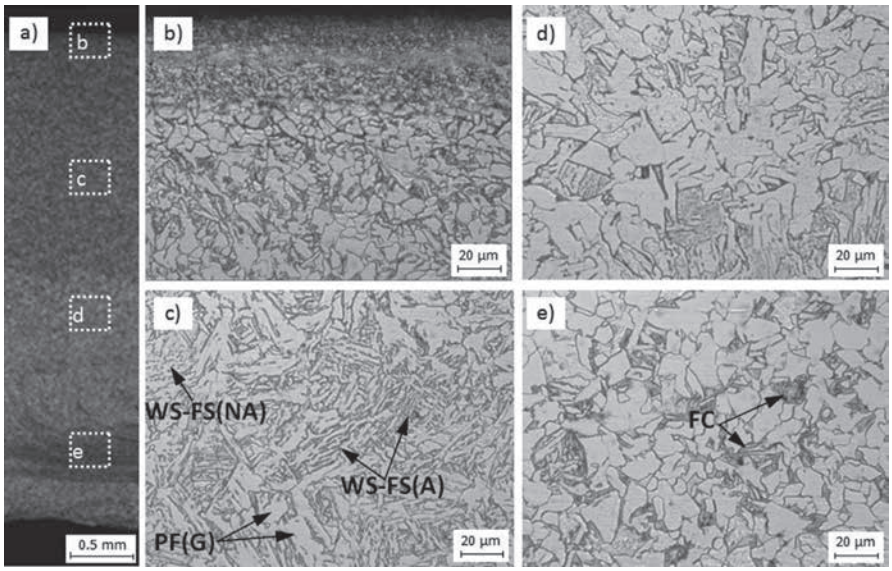


Figure 6: Optical micrographs taken from different regions of the DXZ on a vertical line in the center, a) positions in the DXZ where the following microstructures were taken, b) top region, c), d) mid-sections, e) root region

The optical microscope images given in Figure 6 show the different regions of the DXZ in a vertical direction at the center of DXZ. The microstructures observed in the DXZ of FSWed joint are similar to the microstructures evolving in the weld regions of the fusion welded steel joints. Therefore, they can be classified according to the International Institute of Welding (IIW) [52]. The microstructure observed in the DXZ consists of grain boundary ferrite (PF(G)), oriented Widmanstatten ferrite (WF-FS(A)), random Widmanstatten ferrite (WF-FS(NA)) and ferrite+cementite aggregates (FC). The microstructure in the top region of the DXZ consists of equiaxed fine grains and the upper section of this top region (corresponding to the region just beneath the shoulder of stirring tool), which is about 40 µm in length, has a microstructure consisting of ultra-fine grains (see Figure 6b). Therefore, it can be concluded that there is a grain refinement in this region, which is in contact with the shoulder of the tool during FSW, due to high plastic deformation and subsequent rapid cooling [34].

Figure 6c shows a microstructure consisting of a predominantly Widmanstatten ferrite structure. This microstructure also contains PF(G) and FC. However, distinguishing the FC aggregates formed along the Widmanstatten ferrite lamellae is not easy. The microstructure shown in Figure 6d is the microstructure of the stir zone which contains more PF(G). The microstructure of the TMAZ, which consists of clearly distinguishable FC aggregates, is given in Figure 6e. The stir zone of the joints exhibited a microstructural variation across the vertical direction. This variation in microstructure could not only be explained by the phase transformation and deformation rate although they are very effective as proposed by [48].

Moreover, no clear indication of WC particles due to tool wear has been observed in the microstructure although EDS analyses indicated that there are traces of W in the stir zone of the joints produced. This indicates that tool wear occurs very slowly. It was also observed that the shape of the stirring tool (WC) was damaged after conducting about 3 meters of joining.

Mechanical properties. Figure 7 illustrates the hardness profile of the joint produced in the study as well as a graph show-

Materials Testing downloaded from www.hanser-elibrary.com by Hanser - Library on December 17, 2018
For personal use only.

ing the hardness variation in a vertical line at the center of the stir zone of the joint. Figure 7 also shows the locations of both the horizontal hardness profile and the vertical line along which the hardness measurements were made, as well as the microstructures corresponding to the different locations along the vertical line where the hardness measurements were conducted. Average hardness values of the base plates, namely St 37 and St 44, are 137 HV and 184 HV, respectively.

The hardness profile indicated that the hardness value varies between 258 HV and 228 HV within the DXZ of the joint (see Figure 7b). Moreover, it can also be observed from the hardness profile that there is a sharp decrease in the hardness at the transition region between the DXZ and the HAZ on the retreating side (St 37). The minimum hardness values measured in the TMAZ and HAZ are about 165 HV and 145 HV, respectively. On the other hand, a more gradual decrease in hardness was observed on the advanced side (St 44) and the minimum hardness values for the TMAZ and HAZ were measured at about 215 HV and 195 HV, respectively, which are higher than those on the retreating side. This is reasonable due to the presence of a higher strength St44 steel plate on this side.

The microstructures of the partially or fully grain-refined HAZ regions which consist of ferrite and pearlite phases differ from the microstructures of both base materials. The hardness of these regions was higher than those of the base materials, i. e., St 37 and St 44. This is due to the presence of different microstructures in the HAZ regions and the base materials. The hardness variation in a vertical line from the top to the root regions of the DXZ at the center of the joint is seen in Figure 7d. The hardness values of the upper half section of the joint are higher than those of the lower half section. The hardness values of the upper half section varied from 210 HV to 248 HV. Minimum hardness lies just below the mid-section of the DXZ (in the plate thickness direction). As clearly seen from Figure 7c, the reason for this minimum hardness value was the presence of a coarse grained structure in this region. On the other hand, the highest hardness value was observed in the upper half region just above the mid-section of the joint. The hardness value in this region is higher than that near the top surface of the joint although the finest grained microstructure observed is in this top region. This is due to the presence of a Widmanstatten ferrite structure evolving in the region just above the mid-section.

It can be concluded that the hardness values measured within the weld region are much higher than those of both base plates, indicating that there is a strength overmatching in the weld region. This is due to the microstructural changes taking place in the weld region as discussed above. Similar strength overmatching was also reported for laser beam welded St 37 [54], St 52 [55] and other steels joints [56, 57] due to the phase transformations taking place within the weld region in these joints as well.

Figure 8a shows the stress-strain curves of the transverse tensile test specimens extracted from the joints produced at different rotational rates. Furthermore, the tensile test results obtained were summarized in Table 2. The tensile specimens extracted from the joint produced at a rotational rate of 630 rev × min^{-1} failed far away from the weld region within the St 37 base plate

Sample	Yield strength (MPa)	Tensile strength (MPa)	Strain at fracture (%)
St 44 base plate	280 ± 6	442 ± 2	37 ± 2
St 37 base plate	250 ± 4	373 ± 2	45 ± 1
1000 rpm	225 ± 5	262 ± 4	3 ± 1
800 rpm	310 ± 4	343 ± 4	7 ± 1
630 rpm	275 ± 3	387 ± 2	12 ± 3

Table 2: Tensile test results of the specimens extracted from two base plates and welded joints

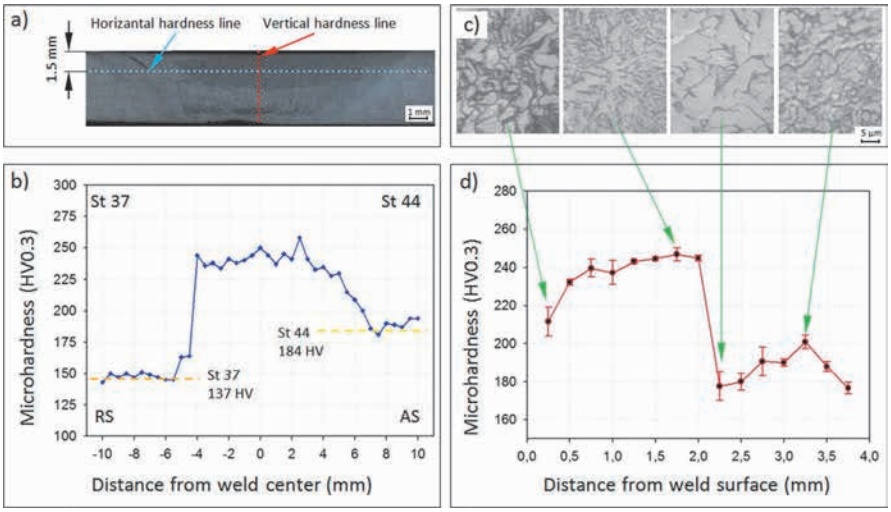


Figure 7: a) Macrograph showing the cross section of the joint produced at a rotational rate of 630 rev × min^{-1} and the locations where microhardness measurements were conducted, b) microhardness profile showing hardness distribution across the weld cross-section, c) microstructures present at the locations where the hardness measurements were conducted in the vertical hardness profile, d) vertical hardness profile showing the hardness variation in a vertical line at the center of the stir zone

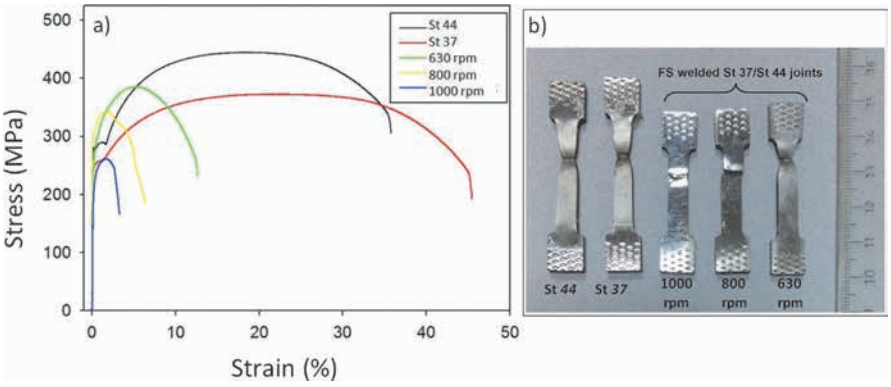


Figure 8: a) Stress-strain curves obtained from three dissimilar joints produced at three different rotational rates, b) failure locations in the specimens

Materials Testing downloaded from www.hanser-elibrary.com by Hanser - Library on December 17, 2018
For personal use only.

side. Thus, the failure mode of this joint is very similar to that of the St 37 base plate, which is ductile, as seen in Figure 8b. Furthermore, it is worth mentioning that although there was a small defect (oxide pick-up from the anvil and a small groove probably due to the sticking of the plates to the anvil during FSW) in the root region of this joint this did not affect the failure location due to the shielding effect resulting from the strength overmatching of the weld nugget. On the other hand, the specimens extracted from the other joints (namely those obtained at a rotational rate of 1000 and 800 rev × min^{-1}) failed just outside the DXZ in a brittle manner (see Figure 8b). The reason for this is the presence of weld defects within the weld region of these two joints as discussed earlier (see Figures 4b and 4c). These results indicate that the crack initiating within the DXZ of these two joints containing a weld defect tries to deviate into the lower strength base metal side (St 37) and failure occurs in the HAZ region before the crack reaches the St 37 side. Similarly, crack deviation into the lower strength side block was also reported in the overmatched dissimilar joints between the pure-Ti side blocks with a higher strength Ti64 alloy interlayer although the crack was originally within the interlayer [58] and dissimilar joints between Ti-Al [59].

Furthermore, as clearly seen from this figure, the specimens obtained at rotational rates of 1000 rev × min^{-1} and 800 rev × min^{-1} failed in a brittle fracture mode, particularly the former. The elongation of the specimens extracted from the joints are 3 %, 7 % and 12 % for the joints at rotational rates of 1000 rev × min^{-1}, 800 rev × min^{-1} and 630 rev × min^{-1}, respectively (see Table 2). Thus, the elongation value increases by decreasing the rotational rate. Moreover, the tensile strength also increases by decreasing the otational rate. The maximum tensile strength value, i. e., 387 MPa, was obtained from specimens extracted from the joint at a rotational rate of 630 rev × min^{-1}. The yield strength of this joint was 275 MPa. These results correspond to 103 % and 110 % of the tensile and yield strengths of the lower strength base plate, i. e., St 37, respectively.

The maximum yield strength, i. e., 310 MPa, was obtained from the joint produced at the lowest rotational rate, i. e., 800 rev × min^{-1}. This is significantly higher than that of the lower strength St 37 base plate (e. g., about 124 %). This joint also exhibited a reasonable tensile strength value, i. e., 343 MPa. However, the elongation of the joint, i. e. 7 %, is much lower than that of the base plates, i. e., 45 % for St37 and 37 % for St 44. On the other hand, the lowest elongation values were exhibited by the joint at the highest rotational rate, i. e., 1000 rev × min^{-1}. This joint displayed a tensile strength of 225 MPa, a yield strength of 262 MPa and an elongation of 3 %. These results correspond to 70, 90 and 6 % of the lower strength St 37 base plate properties, respectively. Insufficient strength and elongation values of the joints at rotational rates of 1000 rev × min^{-1} and 800 rev × min^{-1} are due to weld defects existing in the stir zones of these joints (see Figure 4). It is worth pointing out that the specimens failed away from the stir zone within the lower strength base plate (i. e., St 37) side although some defects existed within the stir zones of these joints. This is caused by the shielding effect resulting from strength overmatching, i. e., higher hardness and strength of the stir zone than that of the St 37 base plate. Similar results were also reported for laser beam welded dissimilar ferritic-austenitic steel joints [55] and friction stir welded brass alloys joints [24] in which a shielding effect was also observed due to strength overmatching.

Conclusions

In this study, St 37 and St 44 plates were butt-joined using the FSW technique at three rotational rates, and the microstructural and mechanical properties of the joints were investigated. The results drawn from this study can be summarized as follows:

- The joint obtained at a rotational rate of 630 rev × min^{-1} did not contain any weld defect and exhibited the best mechanical properties. Thus, sound and robust joints can readily be achieved between St 37 and St 44 structural steel plates if adequate weld parameters are used.
- A recrystallization took place in the SZ of all the FSWed St 37 and St 44 joints due to heat input applied, and plastic deformation occurred during joining. Therefore, a dominantly Widmanstatten ferrite structure was observed in the SZ, although the microstructures of both base plates consist of coarse ferrite and pearlite grains. On the other hand, a fully or partially grain-refined microstructure was observed within the HAZ regions.
- The maximum hardness value (i. e., 258 HV) was measured within the DXZ of the joint produced at the lowest rotational rate, i. e. 630 rev × min^{-1}.
- The tensile test specimens extracted from the joints at rotational rates of 1000 rev × min^{-1} and 800 rev × min^{-1} failed in the brittle fracture mode and displayed an elongation value of 3 % and 7 %, respectively. The highest elongation and tensile strength values were displayed by the specimens extracted from the joint produced at the lowest rotational rate, i. e. 630 rev × min^{-1}.
- The current study clearly demonstrated that structural steel plates with different C-contents can be joined up to 3 meters defect-free by means of FSW and using a WC stirring tool.

References

1 W. M. Thomas, E. D. Nicholas, C. Needham, M. G. Murch, P. Templesmith, C. J. Dawes, International Patent application No. PCT/GB92/02203 and GB Patent application No. 9125978.8 and US Patent application No. 5,460,317 (1991)
2 G. Çam, G. İpekoğlu: Recent developments in joining of aluminum alloys, International Journal of Advanced Manufacturing Technology 91 (2017), No. 5 – 8, pp. 1851-1866 DOI:10.1007/s00170-016-9861-0
3 G. Çam, S. Mistikoglu: Recent developments in friction stir welding of Al-alloys, Journal of Materials Engineering and Performance 23 (2014), No. 6, pp. 1936-1953 DOI:10.1007/s11665-014-0968-x
4 R. Nandan, T. Debroy, H. K. D. H. Bhadeshia: Recent advances in friction-stir welding – Process, weldment structure and properties, Progress in Materials Science 53 (2008), No. 6, pp. 980-1023 DOI:10.1016/j.pmatsci.2008.05.001
5 P. L. Threadgill, A. J. Leonard, H. R. Shercliff, P. J. Withers: Friction stir welding of aluminium alloys, International Materials Reviews 54 (2009), No. 2, pp. 49-93 DOI:10.1179/174328009X411136
6 R. S. Mishra, Z. Y. Ma: Friction stir welding and processing, Materials Science and Engineering: R: Reports 50 (2005), No. 1-, pp. 1-78 DOI:10.1016/j.mser.2005.07.001
7 G. İpekoğlu, B. Gören Kıral, S. Erim, G. Çam: Investigation of the effect of temper condition friction stir weldability of AA7075 Al-alloy plates, Materiali in Tehnologije/Materials and technology 46 (2012), No. 6, pp. 627-632 DOI:669.715 : 621.791 : 620.17
8 Y. Bozkurt, S. Salman, G. Çam: Effect of welding parameters on lap shear tensile properties of dissimilar friction stir spot welded AA 5754-H22/2024-T3 joints, Science and Technology of Welding and Joining 18 (2013), No. 4, pp. 337-345 DOI:10.1179/1362171813Y-0000000111
9 G. İpekoğlu, S. Erim, B. Gören Kıral, G. Çam: Investigation into the effect of temper condition on friction stir weldability of AA6061 Al-alloy plates, Kovove Materialy – Metallic Materials, 51 (2013), No. 3, pp. 155-163 DOI:10.4149/km-2013-3-155

10 G. Çam, S. Güçlüer, A. Çakan, H. T. Serindağ: Mechanical properties of friction stir butt-welded Al-5086 H32 plate, Materialwissenschaft und Werkstofftechnik 40 (2009), No. 8, pp. 638-642 DOI:10.1002/mawe.200800455
11 G. İpekoğlu, S. Erim, G. Çam: Effects of temper condition and post weld heat treatment on the microstructure and mechanical properties of friction stir butt-welded AA7075 Al alloy plates, International Journal of Advanced Manufacturing Technology 70 (2014), No. 1-4, pp. 201-213 DOI:10.1007/s00170-013-5255-8
12 G. İpekoğlu, S. Erim, G. Çam: Investigation into the influence of post-weld heat treatment on the friction stir welded AA6061 Al-alloy plates with different temper conditions, Metallurgical and Materials Transactions A 45 (2014), No. 2, pp. 864-877 DOI:10.1007/s11661-013-2026-y
13 G. İpekoğlu, G. Çam: Effects of initial temper condition and postweld heat treatment on the properties of dissimilar friction-stir-welded joints between AA7075 and AA6061 aluminum alloys, Metallurgical and Materials Transactions A 45 (2014), No. 7, pp. 3074-3087 DOI:10.1007/s11661-014-2248-7
14 G. Çam, G. İpekoğlu, H. T. Serindağ: Effects of use of higher strength interlayer and external cooling on properties of friction stir welded AA6061-T6 joints, Science and Technology of Welding and Joining 19 (2014), No. 8, pp. 715-720 DOI:10.1179/1362171814Y.0000000247
15 B. Çevik, Y. Özçatalbaş, B. Güleç: Effect of tool material on microstructure and mechanical properties in friction stir welding, Materials Testing 58 (2016), No. 1, pp. 36-42, DOI:10.3139/120.110816
16 K. Özel, C. S. Cetinarslan, M. Sahin: Mechanical properties of friction stir welded 5083 aluminum alloys, Materials Testing 59 (2017), No. 1, pp. 64-68 DOI:10.3139/120.110965
17 G. Srinivaso Rao, V. V. Subba Rao, S. R. Koteswara Rao: Mechanical and corrosion properties of friction stir welded joints of Al-Cu alloy 2219-T87, Materials Testing 57 (2015), No. 9, pp. 733-743 DOI:10.3139/120.110775
18 H. T. Serindağ, B. Goren Kiral, Z. A. Kadayifçi: Finite element analysis of friction stir welded aluminum alloy AA6061-T6 joints, Materials Testing 56 (2014), No. 11-12, pp. 937-944 DOI:10.3139/120.110653
19 Ş. Kasman: Effects of FSW parameters and pin geometry on the weldability of EN AW 2024 alloy, Materials Testing 58 (2016), No. 7-8, pp. 694-701 DOI:10.3139/120.110908
20 G. Çam: Friction stir welded structural materials: Beyond Al-alloys, International Materials Reviews 56 (2011), No. 1, pp. 1-48 DOI:10.1179/095066010X12777205875750
21 A. Günen, E. Kanca, M. Demir, F. Çavdar, S. Mistikoğlu, and G. Çam: Microstructural and mechanical properties of friction stir welded pure lead, Indian Journal of Engineering & Materials Sciences (IJEMS) 25 (2018), No. 1, pp. 26-32

Materials Testing downloaded from www.hanser-elibrary.com by Hanser - Library on December 17, 2018
For personal use only.

Abstract

Mechanische Eigenschaften von rührreibgeschweißten Verbindungen der Stähle St 37 und St 44. In der diesem Beitrag zugrunde liegenden Studie wurde die Schweißbarkeit einer Platte eines Stahles St 37 mit einer niedrigeren Festigkeit mit einer Platte aus einem Stahl St 44 mit einer höheren Festigkeit unter Einsatz des Rührreibschweißprozesses (Friction Stir Welding – FSW) untersucht. Bleche aus dem Stahl St 37 werden breitflächig in verschiedenen Industriezweigen verwandt. Allerdings wird ein Verbinden mit Stählen höherer Festigkeit benötigt, wenn die Festigkeit des Stahles St 37 nicht ausreicht. Daher wurden die mikrostrukturellen und mechanischen Eigenschaften von FSW-Stumpfschweißverbindungen des Typs St 37-St 44 untersucht, indem Lichtmikroskopie, Mikrohärtemessungen und Zugversuche angewandt wurden. Es wurde eine feinkristallisierte Mikrostruktur in den Schweißverbindungen beobachtet. Die höchste Zugfestigkeit von 385 MPa ergab sich für die Schweißverbindung, die mit einer Umdrehungsgeschwindigkeit von 630 rev × min^{-1} hergestellt wurde.

22 T. Küçükömeroğlu, E. Şentürk, L. Kara, G. İpekoğlu, G. Çam: Microstructural and mechanical properties of friction stir welded nickel-aluminum bronze (NAB) alloy, Journal of Materials Engineering and Performance 25 (2016), No. 1, pp. 320-326 DOI:10.1007/s11665-015-1838-x
23 G. Çam, S. Mistikoglu, M. Pakdil: Microstructural and mechanical characterization of friction stir butt joint welded 63 % Cu-37 % Zn brass plate, Welding Journal 88 (2009), No. 11, pp. 225 s-232 s
24 G. Çam, H. T. Serindağ, A. Çakan, S. Mıstıkoğlu, H. Yavuz: The effect of weld parameters on friction stir welding of brass plates, Materialwissenschaft und Werkstofftechnik 39 (2008), No. 6, pp. 394-399 DOI:10.1002/mawe.200800314
25 W. M. Thomas, P. L. Threadgill, E. D. Nicholas: Feasibility of friction stir welding steel, Science and Technology of Welding and Joining 4 (1999), No. 6, pp. 365-372 DOI:10.1179/136217199101538012
26 Y. C. Chen, H. Fujii, T. Tsumura, Y. Kitagawa, K. Nakata, K. Ikeuchi, K. Matsubayashi, Y. Michishita, Y. Fujiya, J. Katoh: Friction stir processing of 316L stainless steel plate, Science and Technology of Welding and Joining 14 (2009), No. 3, pp. 197-201 DOI:10.1179/136217108X386527
27 Y. S. Sato, N. Harayama, H. Kokawa, H. Inoue, Y. Tadokoro, S. Tsuge: Evaluation of microstructure and properties in friction stir welded superaustenitic stainless steel, Science and Technology of Welding and Joining 14 (2009), No. 3, pp. 202-209 DOI:10.1179/136217108X386518
28 T. Weinberger, N. Enzinger, H. Cerjak: Microstructural and mechanical characterisation of friction stir welded 15-5PH steel, Science and Technology of Welding and Joining 14 (2009), No. 3, pp. 210-215 DOI:10.1179/136217109X406956
29 M. P. Miles, T. W. Nelson, R. Steel, E. Olsen, M. Gallagher: Effect of friction stir welding conditions on properties and microstructures of high strength automotive steel, Science and Technology of Welding and Joining 14 (2009), No. 3, pp. 228-232 DOI:10.1179/136217108X388633
30 Y. D. Chung, H. Fujii, R. Ueji, K. Nogi: Friction stir welding of hypereutectoid steel (SK5) below eutectoid temperature, Science and Technology of Welding and Joining 14 (2009), No. 3, pp. 233-238 DOI:10.1179/136217109X415901
31 G. Buffa, L. Fratini: Friction stir welding of steels: process design through continuum based FEM model, Science and Technology of Welding and Joining 14 (2009), No. 3, pp. 239-246 DOI:10.1179/136217109X421328
32 H. Fujii, R. Ueji, Y. Takada, H. Kitahara, N. Tsuji, K. Nakata, K. Nogi: Friction stir welding of ultrafine grained interstitial free steels, Materials Transactions 47 (2006), No. 1, pp. 239-241 DOI:10.2320/matertrans.47.239
33 H. Fujii, L. Cui, N. Tsuji, M. Maeda, K. Nakata, K. Nogi: Friction stir welding of carbon steels Materials Science and Engineering A 429 (2006), No. 1-2, pp. 50-57 DOI:10.1016/j.msea.2006.04.118
34 T. J. Lienert, W. L. Stellwag, B. B. Grimmett, R. W. Warke: Friction stir welding studies on mild steel, Welding Journal 82 (2003). No.1, pp. 1s-9s
35 L. Cui , H. Fujii, N. Tsuji, K. Nogi: Friction stir welding of a high carbon steel, Scripta Materialia 56 (2007), No. 7, pp. 637-640 DOI:10.1016/j.scriptamat.2006.12.004
36 M. Imam, R. Ueji, H. Fujii: Microstructural control and mechanical properties in friction stir welding of medium carbon low alloy S45C steel, Materials Science and Engineering A 636 (2015), pp. 24-34 DOI:10.1016/j.msea.2015.03.089 0921-5093
37 L. Cui , H. Fujii, N. Tsuji, K. Nakata, K. Nogi, R. Ikeda, M. Matsushita: Transformation in

stir zone of friction stir welded carbon steels with different carbon contents, ISIJ International 47 (2007), No. 2, pp. 299-306
38 A. Ozekcin, H. W. Jin, J. Y. Koo, N. V. Bangaru, R. Ayer: A microstructural study of friction stir welded joints of carbon steels, International Journal of Offshore and Polar Engineering 14 (2004), No. 4, pp. 284-288
39 G. Çam, G. İpekoğlu, T. Küçükömeroğlu, S. M. Aktarer: Applicability of friction stir welding to steels, Journal of Achievements in Materials and Manufacturing Engineering (JAMME) 80 (2017), No. 2, pp. 65-85, DOI:10.5604/01.3001.0010.2027
40 H. Fujii, L. Cui, K. Nakata, K. Nogi: Mechanical properties of friction stir welded carbon steel joints – friction stir welding with and without transformation, Welding in the World 52 (2008), No. 9-10, pp. 75-81 DOI:10.1007/BF03266672
41 M. J. Russel, C. Blignault, N. L. Horrex, C. S. Wiesner: Recent developments in the friction stir welding of titanium alloys, Welding in the World 52 (2008), No. 9-10, pp. 12-15 DOI:10.1007/BF03266662
42 S. Shashi Kumar, N. Murugan, K. K. Ramachandran: Effect of friction stir welding on mechanical and microstructural properties of AISI 316L stainless steel butt joints, Welding in the World 2018 DOI:10.1007/s40194-018-0621-7
43 H. Kokowa, S. H. C. Park, Y. S. Sato, K. Okamoto, S. Hirano, M. Inagaki: Microstructures in friction stir welded 304 austenitic stainless steel, Welding in the World 49 (2005), No. 3-4, pp. 34-40 DOI:10.1007/BF03266473
44 D. H. Choi, B. W. Ahn, Y. M. Yeon, S. W. C. Park, Y. S. Sato, H. Kokawa, S. B. Jung: Microstructural characterizations following friction stir welding of dissimilar alloys of low- and high-carbon steels, Materials Transactions 52 (2011), No. 7, pp. 1500-1505 DOI:10.2320/matertrans.M2010438
45 M. Ebrahimnia, M. Goodarzi, M. Nouri, M. Sheikhi: Study of the effect of shielding gas composition on the mechanical weld properties of steel St 37-2 in gas metal arc welding, Materials & Design 30 (2009), No. 9, pp. 3891-3895 DOI:10.1016/j.matdes.2009.03.031
46 J. Winczek: Modeling of heat affected zone in multipass gmaw surfacing s235 steel element, Procedia Engineering 136 (2016), pp. 108-113 DOI:10.1016/j.proeng.2016.01.182
47 J. Brnic, G. Turkalj, J. Niu, M. Canadija, D. Lanc: Analysis of experimental data on the behavior of steel S275JR – Reliability of modern design, Mater Des 47 (2013), pp. 497-504 DOI:10.1016/j.matdes.2012.12.037
48 M. Jafarzadegan, A. H. Feng, A. Abdollah-zadeh, T. Saeid, J. Shen, H. Assadi: Microstructural characterization in dissimilar friction stir welding between 304 stainless steel and st37 steel, Materials Characterization 74 (2012), pp. 28-41 DOI:10.1016/j.matchar.2012.09.004
49 A. K. Lakshminarayanan, V. Balasubramanian: Understanding the parameters controlling friction stir welding of AISI 409M ferritic stainless steel, Metals and Materials International 17 (2011), No.6, pp. 969-981 DOI:10.1007/s12540-011-6016-6
50 U. Singarapu, K. Adepu, S. R. Arumalle: Influence of tool material and rotational speed on mechanical properties of friction stir welded AZ31B magnesium alloy, Journal of Magnesium and Alloys 3 (2015), No. 4, pp. 335-344 DOI:10.1016/j.jma.2015.10.001
51 P. L. Threadgill: Terminology in friction stir welding, Science and Technology of Welding and Joining 12 (2007), No. 4, pp. 357-360 DOI:10.1179/174329307X197629
52 G. Thewlis: Classification and quantification of microstructures in steels, Materials Science and Technology 20 (2004), No. 2, pp. 143-160 DOI:10.1179/026708304225010325
53 W. M. Thomas, C. S. Wiesner, D. J. Marks, D. G. Staines: Conventional and bobbin friction stir welding of 12 % chromium alloy steel using composite refractory tool materials, Science and Technology of Welding and Joining 14 (2009), No. 3, pp. 247-253 DOI:10.1179/136217109X415893
54 G. Çam, S. Erim, Ç. Yeni, M. Koçak: Determination of mechanical and fracture properties of laser beam welded steel joints, Welding Journal 78 (1999), No. 6, pp. 193 s-201 s
55 G. Çam, Ç. Yeni, S. Erim, V. Ventzke, M. Koçak: Investigation into properties of laser welded similar and dissimilar steel joints, Science and Technology of Welding and Joining 3 (1998), No. 4, pp. 177-189 DOI:10.1179/stw.1998.3.4.177
56 J. F. Dos Santos, G. Çam, F. Torster, A. Insfran, S. Riekehr, V. Ventzke, M. Koçak: Properties of power beam welded steel, Al-and Ti alloys: Significance of strength mismatch, Welding in the World 44 (2000), No. 6, pp. 42-64
57 G. Çam, M. Koçak, J. F. Dos Santos: Developments in laser welding of metallic materials and characterization of the joints, Welding in the World 43 (1999), No. 2, pp. 13-26
58 M. Koçak, M. Pakdil, G. Çam: Fracture behaviour of diffusion bonded titanium alloys with strength mismatch, Science and Technology of Welding and Joining 7 (2002), No. 4, pp. 187-196 DOI:10.1179/136217102225004220
59 G. Çam, M. Koçak, D. Dobi, L. Heikinheimo, M. Siren: Fracture behaviour of diffusion bonded bimaterial Ti–Al joints, Science and Technology of Welding and Joining 2 (1997), No. 3, pp. 95-101 DOI:10.1179/stw.1997.2.3.95

Bibliography

DOI 10.3139/120.111266
Materials Testing
60 (2018) 12, pages 1163-1170
© Carl Hanser Verlag GmbH & Co. KG
ISSN 0025-5300

The authors of this contribution

Prof. Tevfik Küçükömeroğlu is Professor and is Vice-Dean of the Faculty of Engineering and currently working in the Department of Mechanical Engineering, Faculty of Engineering, Karadeniz Technical University, Trabzon, Turkey.

Semih Mahmut Aktarer is Lecturer at Recep Tayyip Erdoğan University and currently working at the Vocational School of Recep Tayyip Erdoğan University, Rize, Turkey.

Assistant Prof. Güven İpekoğlu is currently working at the newly established Iskenderun Technical University, Hatay, Turkey. His fields of research include solid state welding techniques of structural materials, solid mechanics, and the mechanical behavior of welded joints.

Prof. Gürel Çam is Professor at the Iskenderun Technical University, Hatay, Turkey. He is currently a member of the Editorial Board of Journal of Sci. Technol. Weld. Join. since January 2008 and member of the General Board of Turkish Welding Technology Academy, Istanbul.

Materials Testing downloaded from www.hanser-elibrary.com by Hanser - Library on December 17, 2018
For personal use only.